

# Self Pre-training with Masked Autoencoders for Medical Image Analysis

Lei Zhou<sup>1\*</sup>, Huidong Liu<sup>1</sup>, Joseph Bae<sup>2</sup>, Junjun He<sup>3</sup>,  
Dimitris Samaras<sup>1</sup>, and Prateek Prasanna<sup>2</sup>

<sup>1</sup> Department of Computer Science, Stony Brook University, NY, USA

<sup>2</sup> Department of Biomedical Informatics, Stony Brook University, NY, USA

<sup>3</sup> School of Biomedical Engineering, Shanghai Jiao Tong University, Shanghai, China

**Abstract.** Masked Autoencoder (MAE) has recently been shown to be effective in pre-training Vision Transformers (ViT) for natural image analysis. By performing the pretext task of reconstructing the original image from only partial observations, the encoder, which is a ViT, is encouraged to aggregate contextual information to infer content in masked image regions. We believe that this context aggregation ability is also essential to the medical image domain where each anatomical structure is functionally and mechanically connected to other structures and regions. However, there is no ImageNet-scale medical image dataset for pre-training. Thus, in this paper, we investigate a self pre-training paradigm with MAE for medical images, i.e., models are pre-trained on the same target dataset. To validate the *MAE self pre-training*, we consider three diverse medical image tasks including chest X-ray disease classification, CT abdomen multi-organ segmentation and MRI brain tumor segmentation. It turns out MAE self pre-training benefits all the tasks markedly. Specifically, the mAUC on lung disease classification is increased by 9.4%. The average DSC on brain tumor segmentation is improved from 77.4% to 78.9%. Most interestingly, on the small-scale multi-organ segmentation dataset (N=30), the average DSC improves from 78.8% to 83.5% and the HD95 is reduced by 60%, indicating its effectiveness in limited data scenarios. The segmentation and classification results reveal the promising potential of MAE self pre-training for medical image analysis.

**Keywords:** Masked Autoencoders · Self-supervised Learning · Segmentation.

## 1 Introduction

Within a medical image, each anatomical structure is functionally and mechanically connected to other structures and regions present in the human body. As a result, image analysis tasks including classification and segmentation must account for these interdependencies and relationships. For instance, classification of a disease on chest x-ray might rely not only on textural changes within

---

\* Corresponding author, [leizhou@cs.stonybrook.edu](mailto:leizhou@cs.stonybrook.edu)

lung regions but also on relative changes in lung, parenchymal, and mediastinal structures. For segmentation, features inherent to both the target object and surrounding tissue enable delineation of specific structures. The presence of a brain tumor commonly results in additional changes to the tumor’s surrounding environment including the presence of edema, structural shifts in brain tissue, and increased vascularization. We hypothesize that enforcing a strict requirement on contextual information learning can improve deep learning-based medical image analysis.

Recent advancements in self-supervised representation learning show masked image modeling (MIM) [3,24,8,11] as an effective pre-training strategy for the Vision Transformer (ViT) [7], which is powerful yet hard to train because of lack of inductive bias. The basic idea of MIM is *masking* and *reconstructing*: *masking* a set of image patches before input into the transformer and *reconstructing* these masked patches at the output. MIM encourages the network to *infer the masked target by aggregating information from the context*. This ability to aggregate contextual information is essential for vision tasks as well as medical image tasks. Among the different MIM frameworks, Masked Autoencoder (MAE) [11] is one of the most simple and effective.

In this paper, we investigate a MAE-based self pre-training paradigm for medical image analysis tasks. As there is no ImageNet-scale universal medical image dataset, MAE pre-training is performed on the same dataset as the downstream task. We term this *self pre-training*. We conduct experiments on three diverse medical image tasks including lung disease classification on chest X-ray14 (CXR14 [23]), CT multi-organ segmentation on BTCV [14] and MRI brain tumor segmentation (BRATS) from Medical Segmentation Decathlon Challenge [1]. These three datasets are diverse in task types (classification and segmentation) and imaging modalities (X-rays, CT, and MRI). For all tasks, we take ViT-B/16 [7] as the backbone network. After MAE pre-training, ViT-B/16 is added with a task-specific head. For classification, the head is a simple linear classifier. For segmentation, we follow the decoder design of UNETR [10] which is a recently-proposed segmentation framework with a ViT encoder and a “U-shaped”[19] architecture.

Our results indicate that MAE self pre-training can significantly improve medical image segmentation and classification performance and surpass the ImageNet pre-training paradigm on all the datasets. We also demonstrate that MAE pretraining aids in limited data scenarios.

## 2 Methodology

### 2.1 Preliminary: Vision Transformer

We use ViT as the backbone architecture for both pre-training and downstream tasks. A ViT is composed of the patch embedding layer, position embedding, and Transformer blocks.

**Patch Embedding:** Since a ViT takes a sequence as input, the patch embedding layer needs to transform any high-dimensional data into sequences. For a

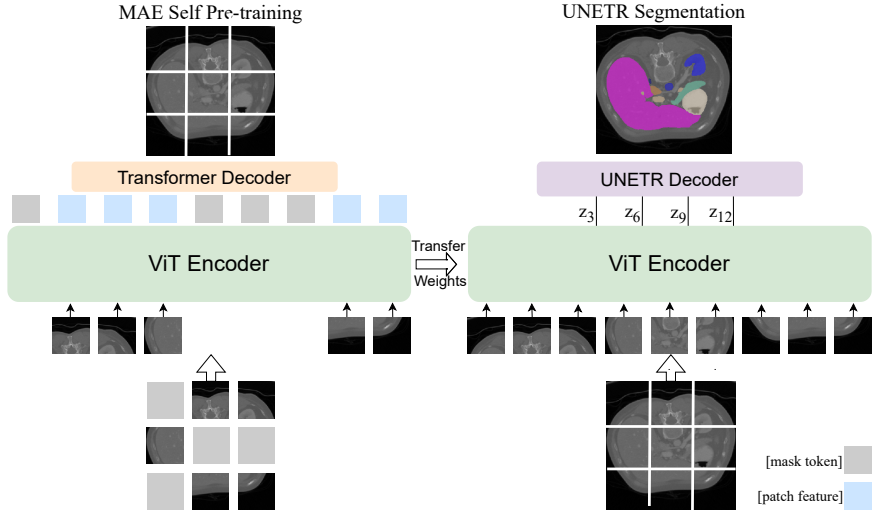


**Fig. 1.** Pipeline for Segmentation with MAE Self Pre-training. In the first stage (shown in the left), ViT is pre-trained with MAE as the encoder. ViT encoder is input with a random subset of patches and appended with a transformer decoder to reconstruct the full image. In the second stage (shown in the right), the pre-trained ViT weights are transferred to initialize the segmentation encoder. Then, the whole segmentation network, e.g., UNETR, is finetuned to perform the segmentation task.

3D volume  $\mathbf{x} \in \mathbb{R}^{H \times W \times D \times C}$ , it is first reshaped into a sequence of flattened 3D patches  $\mathbf{x}_p \in \mathbb{R}^{N \times (P^3 \cdot C)}$ , where  $C$  is the input channel,  $(H, W, D)$  is the input resolution,  $(P, P, P)$  is the patch resolution, and  $N = HWD/P^3$  is the number of patches, i.e., the length of the input sequence fed into the Transformer. A trainable linear projection is then applied to map them to patch embeddings.

**Position Embedding:** To retain positional information, patch embeddings are added with position embeddings. The standard ViT adopts 1D learnable position embeddings. However, we experimentally find that the learnable 1D position embeddings can hurt the reconstruction performance of MAE. Therefore, we use the sine-cosine version of position embedding in the pre-training stage. For the downstream tasks, we still adopt the learnable position embedding design but initialize it with sine-cosine embedding values.

**Transformer Block:** A Transformer block consists of alternating layers of multiheaded self-attention (MSA) [21] and MLP blocks.

$$\mathbf{z}'_l = \text{MSA}(\text{LN}(\mathbf{z}_{l-1})) + \mathbf{z}_{l-1}; \quad \mathbf{z}_l = \text{MLP}(\text{LN}(\mathbf{z}'_l)) + \mathbf{z}'_l \quad (1)$$

where  $l$  ranges from 1 to  $L$ , i.e., the number of Transformer blocks, LN is LayerNorm and  $\mathbf{z}_l$  denotes the feature map of the  $l_{th}$  block.

## 2.2 Self Pre-training with Masked Autoencoders

In this section, we illustrate the encoder, decoder and loss function in MAE.

**Encoder in MAE.** The input image/volume is first divided into non-overlapping patches. The patches are then randomly grouped into visible ones and masked ones. The encoder in MAE, i.e., a ViT, only operates on the visible patches. Unlike other MIM methods [3,24], MAE introduces no mask tokens into the encoder which saves computation and speeds up pre-training.

**Decoder in MAE.** The decoder in MAE is input with the full set of tokens including patch-wise representations from the encoder and learnable mask tokens put in the positions of masked patches. By adding positional embeddings to all the input tokens, the decoder can restore the patches in each specific masked position. To reduce the pre-training budget, the decoder is designed to be more lightweight. Note that the decoder is only an auxiliary part used for pre-training and will not be used in downstream tasks.

**Loss function in MAE.** MAE is trained with a reconstruction loss, i.e., mean squared error, by predicting the pixel/voxel values of the masked patches. In practice [11], normalized pixel/voxel values within each patch are better reconstruction targets than raw pixel/voxel values.

## 2.3 Architectures for Downstream Tasks

After MAE self pre-training, we append task-specific heads after ViT to perform downstream tasks, introduced next.

**Linear Layer for Classification.** Following [7], we append a linear classifier after the class token output from ViT. As a chest X-ray can carry more than one label, we finetune the whole network with a binary cross entropy loss.

**UNETR for Segmentation.** We build UNETR [10] upon the MAE pre-trained ViT encoder and a randomly-initialized convolutional decoder. UNETR is recently proposed for 3D image segmentation tasks such as brain tumor segmentation. Its architecture shares the same idea of U-Net [19], i.e. features from multiple resolutions of the encoder are skip-connected with the decoder. The input to the UNETR decoder is a sequence of representations, i.e.,  $\{z_3, z_6, z_9, z_{12}\}$ , from the encoder. Each representation is reshaped to restore the spatial dimension of  $\frac{H}{P} \times \frac{W}{P} \times \frac{D}{P} \times K$  where  $K$  is the feature channel.

Starting from the deepest feature  $z_{12}$ , each representation is applied with a variable number of deconvolutional blocks to increase the resolution by a specific factor ( $\times 2$  for  $z_{12}$  and  $z_9$ ,  $\times 4$  for  $z_6$ , and  $\times 8$  for  $z_3$ ). Then representations of the same spatial resolution, e.g.,  $z_{12}$  and  $z_9$ , are concatenated and further upsampled to match the shape of a shallower feature. Such concatenation and upsampling are repeated until the full resolution of input is restored. Finally, the output layer takes both the upsampled feature and the original full-resolution input to predict a segmentation map.

### 3 Experiments and Results

Experiments on all tasks include two stages: the MAE pre-training and the downstream task. Specifically, a ViT is first pre-trained by MAE on the target dataset. Then, the pre-trained ViT is appended with a task-specific head, i.e., linear layer for classification and UNETR decoder for segmentation. The whole network is finetuned further to perform the downstream task. We consider three diverse tasks for validating MAE for medical images, introduced next.

**Lung Disease Classification on ChestX-ray14.** ChestX-ray14 [23] is a large-scale CXR database consisting of 112,120 frontal-view CXRs from 32,717 patients. We conduct the classification task based on the official split which consists of trainval( $\sim 80\%$ ) and testing ( $\sim 20\%$ ) sets. Because each image can have multiple labels, we adopt the multi-class AUC as the performance metric.

**Abdomen Multi-organ Segmentation on BTCV.** The BTCV [14] (Multi Atlas Labeling Beyond The Cranial Vault) dataset consists of 30 subjects with abdominal CT scans where 13 organs were annotated under the supervision of clinical radiologists. Each CT volume has  $85 \sim 198$  slices of  $512 \times 512$  pixels, with a voxel spatial resolution of  $(0.54 \times 0.98 \times [2.5 \sim 5.0] \text{ mm}^3)$ . For the convenience of comparison, we follow [5] to split the 30 cases into 18 for training and 12 for validation in the same way as [4]. We report the average DSC and 95% Hausdorff Distance on 8 abdominal organs (aorta, gallbladder, spleen, left kidney, right kidney, liver, pancreas, spleen, stomach) to align with [5].

**Brain Tumor Segmentation on MSD.** Brain tumor segmentation is one of the 10 tasks in Medical Segmentation Decathlon (MSD) Challenge [1]. The entire set has 484 multi-modal (FLAIR, T1w, T1-Gd and T2w) MRI brain scans. The ground-truth labels of segmentation includes peritumoral edema, GD-enhancing tumor and the necrotic/non-enhancing tumor core. The performance is measured on three recombined regions, i.e., tumor core, whole tumor and enhancing tumor. We randomly split the dataset into training (80%) and validation (20%) sets. Reported metrics include average DSC and 95% Hausdorff Distance.

#### 3.1 Implementation Details

Our experiments are implemented on PyTorch [17] and MONAI [16]. We use ViT-B/16 as the backbone and utilize the AdamW optimizer in all the experiments. The patch size is  $16 \times 16$  for 2D images and  $16 \times 16 \times 16$  for 3D volumes.

**Data Preprocessing and Augmentation.** For ChestX-ray14, we perform a histogram equalization on all the X-ray images. During training, we randomly flip and crop a  $224 \times 224$  region out of the original  $256 \times 256$  image. For BTCV, we clip the raw values between -175 and 250, and re-scale the range between 0 and 1. During training, we randomly flip and crop a  $96 \times 96 \times 96$  3D volume as the input. For BRATS, we perform an instance-wise normalization over the non-zero region per channel. During training, we randomly flip and crop a  $128 \times 128 \times 128$  3D volume as the input.

**MAE Pre-training.** We use a learning rate of 1.5e-4 and weight decay of 0.05 for all datasets. The pre-training epochs vary. MAE pre-training is run for 800

epochs on ChestX-ray14, 10,000 epochs on BTCV, and 500 epochs on BRATS.

**Task Finetuning.** For all downstream tasks, we adopt a strategy of layer-wise learning rate decay to stabilize the ViT training and a random DropPath with a 10% probability. The learning rates vary between tasks. The learning rate is 1e-3 for lung disease classification, 8e-4 for multi-organ segmentation, and 4e-4 for brain tumor segmentation.

### 3.2 Results

**MAE Reconstruction.** We show the reconstruction results of MAE with a

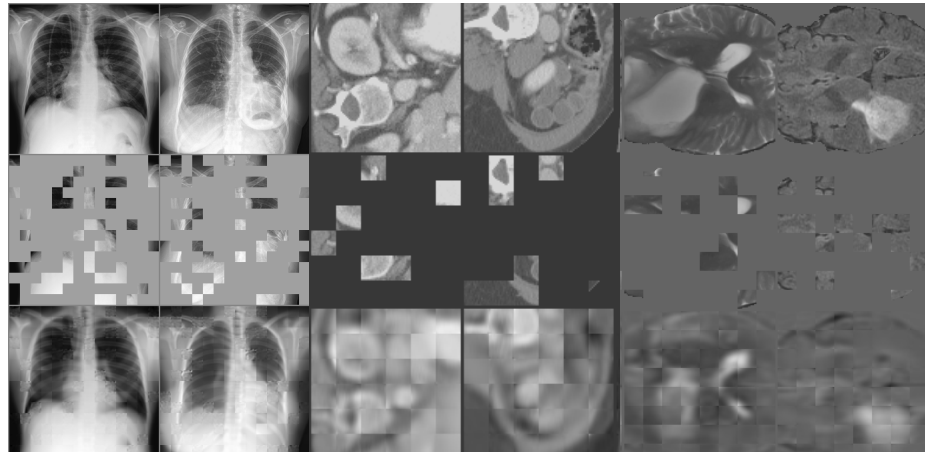


**Fig. 2.** MAE reconstruction results. The first row is the original image, the second row is the masked image where masked region is denoted by gray or black patches. The third row the reconstruction of MAE from the unmasked patches. Every two columns show the results of one dataset, i.e., CXR, BTCV and BRATS from left to right.

mask ratio of 75% in Fig 2. The three rows show the original images, the masked images, and the reconstructed images. The results show that MAE is able to restore the lost information from the random context. As the reconstruction loss is only applied to the masked patches, the restored visible patches look blurrier, which is also observed in the natural images [11]. It is worth noting that the ultimate goal of MAE is to benefit the downstream tasks instead of generating high-quality reconstructions.

**Lung Disease Classification.** To validate the effectiveness of MAE self pre-training, we compare the MAE self pre-trained ViT-B/16 with several different methods, including training from scratch, longer training, and training with transferred ImageNet weights. The results are listed in Table 1. First, with no pre-training, ViT hardly achieves a competitive result even with long training

epochs. This is expected considering its large model size and lack of inductive bias. Second, MAE self pre-training outperforms the ImageNet pre-trained ViT by 0.8%. This shows the promising potential of the new MAE self pre-training paradigm for medical images. Finally, we compare with the CNN-based SOTA using both ImageNet pre-training and self-supervised pre-training by MoCo [12,6] and LSAE [26]. ViT with MAE self pre-training outperforms them all.

**Table 1.** Lung Disease Classification on ChestX-ray14.

Architectures	Pre-training		Epochs	mAUC
	Method	Dataset		
CXR14-R50 [23]	supervised	ImageNet-1K	-	74.5%
ChestNet [22]	supervised	ImageNet-1K	-	78.1%
CheXNet [18][25]	supervised	ImageNet-1K	-	78.9%
ResNet18 [13]	MoCo [12]	Self	-	78.6%
ResNet50	MoCo-v2 [6]	Self	-	79.4%
$Enc_t$ [25]	LSAE	self	-	79.0%
ViT-B/16	None	None	100	74.4%
ViT-B/16	None	None	400	74.9%
ViT-B/16	supervised	ImageNet-1K	100	80.7%
ViT-B/16	MAE	Self	100	<b>81.5%</b>

**Abdomen Multi-organ Segmentation.** The results are shown in Table 2. First, we reproduce the UNETR baseline with an average DSC of 78.83% on BTCV. Then, after MAE self pre-training, we initialize the encoder with the pre-trained weights and the decoder randomly. The whole UNETR is finetuned to perform the multi-organ segmentation task. Both UNETR and UNETR with MAE surpass the other SOTA methods. Most importantly, MAE self pre-training improves upon the UNETR baseline by a large margin, from 78.8% to 83.5% on average DSC. It is also superior to the ImageNet pre-training paradigm. As MAE is previously only applied on large-scale datasets like ImageNet (N=1000,000), it is interesting to observe its notable performance on a small-scale dataset (N=30); this further demonstrates the promising potential of applying MAE self pre-training to medical images in limited data scenarios.

**Brain Tumor Segmentation.** Similar to multi-organ segmentation, we also use UNETR as our segmentation baseline for the brain tumor segmentation task. Results are listed in Table 3. UNETR achieves an average DSC of 77.4% and a HD95 of 7.78mm. With the help of MAE (12.5% mask ratio) self pre-training, the performance of UNETR is improved further achieving a 78.91% DSC and a HD95 of 7.22mm.

**Ablation Study.** In Table 4, we conduct experiments with different MAE pre-training epochs and mask ratios. First, the performance of MAE on BRATS benefits from longer training though this is not the case for BTCV. Second, unlike the high mask ratio [11] adopted in natural images, the two segmentation

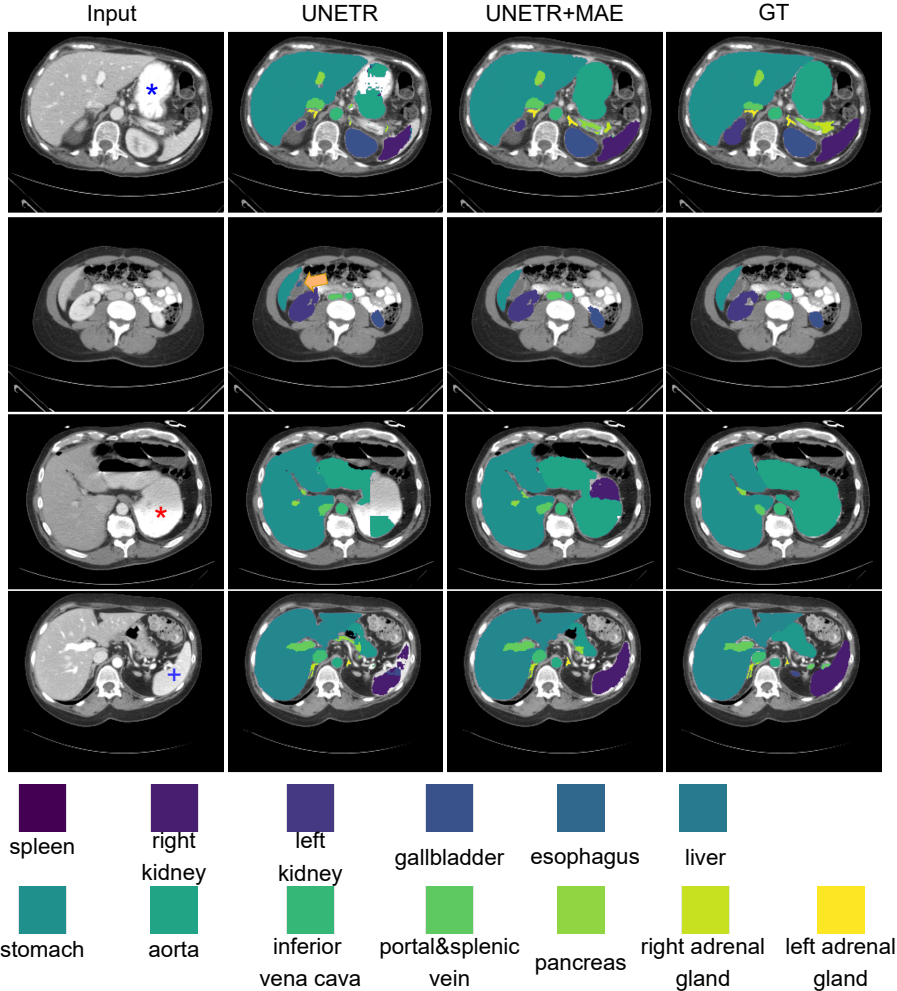


**Fig. 3.** Qualitative Results of Abdomen Multi-organ Segmentation on BTCV. The displayed results for four different images demonstrate qualitative examples of improved performance when UNETR is pre-trained with MAE for abdominal organ segmentation. Note in the first row, the stomach segmentation (blue asterisk) is incomplete when created by the baseline UNETR approach compared to the segmentation produced by an MAE pre-trained UNETR architecture. In the second row the absence of the false positive segmentation (orange arrow). In the third row there is a more complete segmentation of the organ denoted with the red asterisk when UNETR is pre-trained with MAE. Finally, in the fourth row, note the increased segmentation of the spleen (denoted by the blue cross). These improvements in segmentation are in agreement with the quantitative results described previously in this paper.

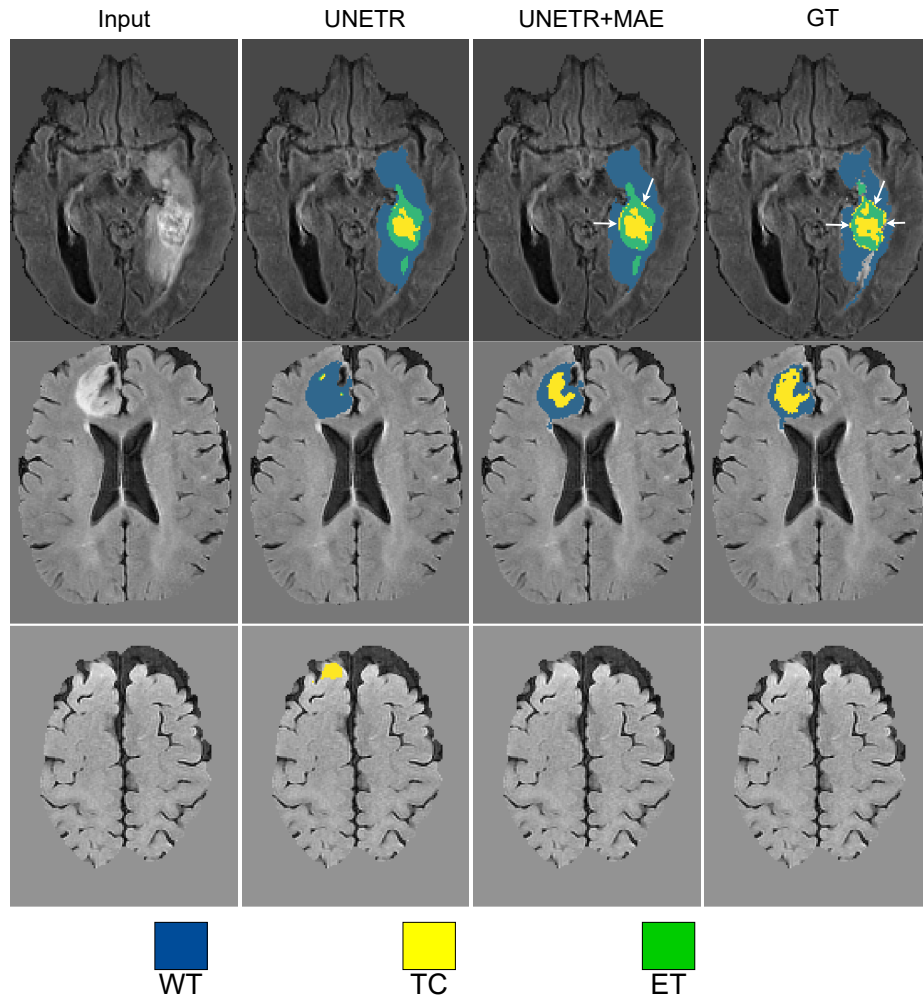


**Fig. 4.** Qualitative Results of Brain Tumor Segmentation on MSD. Qualitative brain tumor segmentation results displayed here demonstrate improvement in segmentation results when UNETR is pre-trained with MAE. In the first row, only subtle improvements are noticeable in the segmentation such as peripheral yellow necrotic core segmentations (white arrows) being captured after MAE pre-training. In the second and third rows, improvements are more obvious. Necrotic core segmentations nearly absent without MAE pre-training in row 2, and false positive necrotic core segmentations appear without pre-training in row 3.

tasks show different preference to the mask ratio. With a decrease in mask ratio from 87.5% to 12.5%, both segmentation tasks are consistently improved.

**Table 2.** Abdomen Multi-organ Segmentation on BTCV

Framework	Avg	DSC/HD95	Aorta	Gallbladder	Kidney(L)	Kidney(R)	Liver	Pancreas	Spleen	Stomach
V-Net [15]		68.81/-	75.34	51.87	77.10	80.75	87.84	40.05	80.56	56.98
DARR [9]		69.77/-	74.74	53.77	72.31	73.24	94.08	54.18	89.90	45.96
U-Net(R50) [19]		74.68/36.87	84.18	62.84	79.19	71.29	93.35	48.23	84.41	73.92
AttnUNet(R50) [20]		75.57/36.97	55.92	63.91	79.20	72.71	93.56	49.37	87.19	74.95
TransUNet [5]		77.48/31.69	87.23	63.13	81.87	77.02	94.08	55.86	85.08	75.62
UNETR		78.83/25.59	85.46	70.88	83.03	82.02	95.83	50.99	88.26	72.74
UNETR+ImageNet		79.67/24.28	86.07	74.29	82.44	81.65	95.84	58.08	87.74	69.98
UNETR+MAE		<b>83.52/10.24</b>	<b>88.92</b>	<b>75.25</b>	<b>86.37</b>	<b>84.00</b>	<b>95.95</b>	<b>65.02</b>	<b>90.56</b>	<b>80.89</b>

**Table 3.** MSD Brain Tumor Segmentation

Method	Average		WT		ET		TC	
	DSC	HD95	DSC	HD95	DSC	HD95	DSC	HD95
UNETR	77.40	7.78	90.25	<b>6.79</b>	61.45	8.33	80.51	7.57
UNETR+ImageNet	77.78	7.38	90.34	7.19	62.23	7.86	80.78	<b>7.00</b>
UNETR+MAE	<b>78.91</b>	<b>7.22</b>	<b>90.84</b>	7.04	<b>63.88</b>	<b>7.15</b>	<b>82.00</b>	7.13

**Table 4.** Ablation Study on Mask Ratios and Pre-training Epochs. Left: MSD Brain Tumor Segmentation Dataset. Right: BTCV Multi-organ Segmentation Dataset

Mask ratio	Pre-train Epochs	Avg	DSC	WT	ET	TC	Mask ratio	Pre-train Epochs	Avg	DSC
87.5%	500	77.14	90.22	61.06	80.15		87.5%	10k	82.21	
75%	500	78.14	90.60	62.48	81.35		75%	10k	82.76	
75%	1000	78.29	90.25	63.06	81.55		75%	40k	81.09	
75%	2000	78.43	90.33	63.45	81.52					
50%	500	78.42	90.59	63.05	81.63		50%	10k	83.2	
25%	500	78.71	90.76	63.48	81.88		25%	10k	83.18	
12.5%	500	<b>78.91</b>	<b>90.84</b>	<b>63.88</b>	<b>82.00</b>		12.5%	10k	<b>83.52</b>	

## 4 Conclusion

Here we have demonstrated that MAE pre-training improves SOTA classification and segmentation performance on a diverse set of medical image analysis tasks. Of relevance to medical imaging, MAE self pre-training outperforms existing methods on small datasets, including ImageNet-transfer learning. Furthermore,

we demonstrate the effectiveness of MAE on 3D medical images including both CTs and MRIs, something that has not previously been explored. Our ablation results also suggest that parameters including mask ratio and pre-training epochs should be tailored when applying MAE pre-training to the medical imaging domain. Together, these observations suggest that MAE can further improve the already impressive performance of ViTs in medical imaging analysis tasks including classification and segmentation. In future work, we will test the efficacy of MAE pretraining in prognosis and outcome prediction tasks [2].

## References

1. Antonelli, M., Reinke, A., Bakas, S., Farahani, K., Landman, B.A., Litjens, G., Menze, B., Ronneberger, O., Summers, R.M., van Ginneken, B., et al.: The medical segmentation decathlon. arXiv preprint arXiv:2106.05735 (2021)
2. Bae, J., Kapse, S., Singh, G., Gattu, R., Ali, S., Shah, N., Marshall, C., Pierce, J., Phatak, T., Gupta, A., et al.: Predicting mechanical ventilation and mortality in covid-19 using radiomics and deep learning on chest radiographs: A multi-institutional study. *Diagnostics* **11**(10), 1812 (2021)
3. Bao, H., Dong, L., Wei, F.: Beit: Bert pre-training of image transformers. arXiv preprint arXiv:2106.08254 (2021)
4. Chen, J.N.: Transunet, <https://github.com/Beckschen/TransUNet>
5. Chen, J., Lu, Y., Yu, Q., Luo, X., Adeli, E., Wang, Y., Lu, L., Yuille, A.L., Zhou, Y.: Transunet: Transformers make strong encoders for medical image segmentation. arXiv preprint arXiv:2102.04306 (2021)
6. Chen, X., Fan, H., Girshick, R., He, K.: Improved baselines with momentum contrastive learning. arXiv preprint arXiv:2003.04297 (2020)
7. Dosovitskiy, A., Beyer, L., Kolesnikov, A., Weissenborn, D., Zhai, X., Unterthiner, T., Dehghani, M., Minderer, M., Heigold, G., Gelly, S., et al.: An image is worth 16x16 words: Transformers for image recognition at scale. arXiv preprint arXiv:2010.11929 (2020)
8. El-Nouby, A., Izacard, G., Touvron, H., Laptev, I., Jegou, H., Grave, E.: Are large-scale datasets necessary for self-supervised pre-training? arXiv preprint arXiv:2112.10740 (2021)
9. Fu, S., Lu, Y., Wang, Y., Zhou, Y., Shen, W., Fishman, E., Yuille, A.: Domain adaptive relational reasoning for 3d multi-organ segmentation. In: International Conference on Medical Image Computing and Computer-Assisted Intervention. pp. 656–666. Springer (2020)
10. Hatamizadeh, A., Tang, Y., Nath, V., Yang, D., Myronenko, A., Landman, B., Roth, H.R., Xu, D.: Unetr: Transformers for 3d medical image segmentation. In: Proceedings of the IEEE/CVF Winter Conference on Applications of Computer Vision. pp. 574–584 (2022)
11. He, K., Chen, X., Xie, S., Li, Y., Dollár, P., Girshick, R.: Masked autoencoders are scalable vision learners. arXiv preprint arXiv:2111.06377 (2021)
12. He, K., Fan, H., Wu, Y., Xie, S., Girshick, R.: Momentum contrast for unsupervised visual representation learning. In: Proceedings of the IEEE/CVF Conference on Computer Vision and Pattern Recognition. pp. 9729–9738 (2020)
13. He, K., Zhang, X., Ren, S., Sun, J.: Deep residual learning for image recognition. In: Proceedings of the IEEE conference on computer vision and pattern recognition. pp. 770–778 (2016)

14. Landman, B., Xu, Z., Igelsias, J., Styner, M., Langerak, T., Klein, A.: Miccai multi-atlas labeling beyond the cranial vault—workshop and challenge. In: Proc. MICCAI Multi-Atlas Labeling Beyond Cranial Vault—Workshop Challenge. vol. 5, p. 12 (2015)
15. Milletari, F., Navab, N., Ahmadi, S.A.: V-net: Fully convolutional neural networks for volumetric medical image segmentation. In: 2016 fourth international conference on 3D vision (3DV). pp. 565–571. IEEE (2016)
16. MONAI Consortium: MONAI: Medical Open Network for AI (3 2020). <https://doi.org/10.5281/zenodo.4323058>, <https://github.com/Project-MONAI/MONAI>
17. Paszke, A., Gross, S., Massa, F., Lerer, A., Bradbury, J., Chanan, G., Killeen, T., Lin, Z., Gimelshein, N., Antiga, L., et al.: Pytorch: An imperative style, high-performance deep learning library. *Advances in neural information processing systems* **32** (2019)
18. Rajpurkar, P., Irvin, J., Zhu, K., Yang, B., Mehta, H., Duan, T., Ding, D., Bagul, A., Langlotz, C., Shpanskaya, K., et al.: Chexnet: Radiologist-level pneumonia detection on chest x-rays with deep learning. *arXiv preprint arXiv:1711.05225* (2017)
19. Ronneberger, O., Fischer, P., Brox, T.: U-net: Convolutional networks for biomedical image segmentation. In: International Conference on Medical image computing and computer-assisted intervention. pp. 234–241. Springer (2015)
20. Schlemper, J., Oktay, O., Schaap, M., Heinrich, M., Kainz, B., Glocker, B., Rueckert, D.: Attention gated networks: Learning to leverage salient regions in medical images. *Medical image analysis* **53**, 197–207 (2019)
21. Vaswani, A., Shazeer, N., Parmar, N., Uszkoreit, J., Jones, L., Gomez, A.N., Kaiser, Ł., Polosukhin, I.: Attention is all you need. *Advances in neural information processing systems* **30** (2017)
22. Wang, H., Xia, Y.: Chestnet: A deep neural network for classification of thoracic diseases on chest radiography. *arXiv preprint arXiv:1807.03058* (2018)
23. Wang, X., Peng, Y., Lu, L., Lu, Z., Bagheri, M., Summers, R.M.: Chestx-ray8: Hospital-scale chest x-ray database and benchmarks on weakly-supervised classification and localization of common thorax diseases. In: Proceedings of the IEEE conference on computer vision and pattern recognition. pp. 2097–2106 (2017)
24. Xie, Z., Zhang, Z., Cao, Y., Lin, Y., Bao, J., Yao, Z., Dai, Q., Hu, H.: Simmim: A simple framework for masked image modeling. *arXiv preprint arXiv:2111.09886* (2021)
25. Zhou, L., Bae, J., Liu, H., Singh, G., Green, J., Gupta, A., Samaras, D., Prasanna, P.: Lung swapping autoencoder: Learning a disentangled structure-texture representation of chest radiographs. *arXiv preprint arXiv:2201.07344* (2022)
26. Zhou, L., Bae, J., Liu, H., Singh, G., Green, J., Samaras, D., Prasanna, P.: Chest radiograph disentanglement for covid-19 outcome prediction. In: International Conference on Medical Image Computing and Computer-Assisted Intervention. pp. 345–355. Springer (2021)